International Journal of Environment and Geoinformatics 10(4):001-016 (2023)

Research Article

Evaluation of rockfall hazard based on UAV technology and 3D Rockfall Simulations

Mustafa Utlu[1, *], Muhammed Zeynel Öztürk[2], Mesut Şimşek[3], Mehmet Fatih Akgümüş[4]

[1] Department of Geography, Faculty Science and Letter, Bingol University, Bingöl, Türkiye
[2] Department of Geography, Faculty Science and Letter, Niğde Ömer Halis Demir University, Niğde Türkiye
[3] Department of Geography, Faculty Science and Letter, Hatay Mustafa Kemal University, Hatay, Türkiye
[4] Department of Geography, Graduate School of Social Sciences, Ankara University, Ankara, Türkiye

* Corresponding author: M. Utlu
* E-mail: utlumus@gmail.com

Received 06.07.2023
Accepted 10.10.2023

How to cite: Utlu et al., (2023). Evaluation of rockfall hazard based on UAV technology and 3D Rockfall Simulations, *International Journal of Environment and Geoinformatics (IJEGEO)*, 10(4):001-016. doi. 10.30897/ijegeo.10323768

Abstract

Hacıabdullah village, where rockfall events occur frequently, is an important mountainous region located within the boundaries of Niğde province, which is one of the top provinces in Turkey in terms of rockfall events and is located in the Central Anatolia Region. Despite the frequent occurrence of many rockfall events of varying sizes, no precautions are taken as a result of these events, leading to economic damages. Therefore, Hacıabdullah village, which poses a high danger and risk in terms of slope instability and rockfall potential, has been selected as the study area. The study aims to evaluate rockfall events occurring on steep slopes in Hacıabdullah village, based on the potential rock blocks that could fall, by modeling them according to their geometries. Within this scope, the potential 17 rock blocks that could fall have been identified in the field and modelled using RAMMS 3D rockfall software according to their geometric characteristics. For the 3D modeling of the study, UAV-DSM (3cm resolution), which represents the high-resolution surface of the topography, has been used as the main dataset. As a result of 3D rockfall modelling, the maximum kinetic energy, maximum velocity, and maximum jump height of the falling blocks reached 3476 kJ, 23.1 m/s, and 14.57 m, respectively. The result of the kinematic analysis showed a higher probability of toppling type in the whole study area. Rocks that do not move very far from the source area are; in other words, and may significantly damage the roads. However, rolling blocks, in other words, blocks that can travel long distances from the source area, have the potential to cause great damage to the settlement areas, roads, and trees. According to the hazard map, blocks involve high and moderate levels of risk for settlement units.

Keywords: Rockfall, Hazard, RAMMS, 3D modelling, UAV

Introduction

Rockfalls are a common phenomenon in mountainous regions, characterized by their high velocity and destructive potential and one of the most dangerous natural disasters experienced on earth (Liu et al. 2021; Graber and Santi 2022). Rockfalls represent a considerable hazard to human-related activities, particularly in the vicinity of railways, roads, and critical infrastructure as well as human life (Lu et al. 2019; Schilirò et al. 2022). Their hazardousness arises from the inherent difficulty in predicting their occurrence due to the multifaceted factors that trigger them, including weather, seismic activity, erosion, and anthropogenic actions. Moreover, the absence of apparent precursors prior to their collapse renders rockfalls challenging to anticipate and prepare for. These events involve blocks of rock moving downhill through a combination of free-fall, rolling, bouncing, and sliding, often resulting in fragmentation and scattering of the material across the slope (Liu et al. 2021; Feng et al. 2021). Thus, rockfalls possess several menacing attributes, including their frequent occurrence and the mobilization of large blocks over extended distances, which can be attributed to their high kinetic energy and velocity (Hungr et al. 2014; Farvacque et al. 2019; Yin et al. 2023). Rockfalls are a common hazard, particularly in settlements on steep slopes or mountainous areas. These events occur when large rocks or boulders break loose from the face of a cliff or slope and tumble down the mountainside. The exact location of these events can vary widely, but they are more likely to occur in areas with unstable rock formations or other geological features that increase the risk of rockfall (Michoud et al. 2012; Giordan et al. 2015). In the rock blocks where free fall, jumping, and rolling motion types are observed in fields with a topographic inclination of 30° and 90°, the size of the rock blocks generally varies between 1-100 m³, and their speed varies between 1-10 m/s (Ritchie 1963; Fanos ve Pradhan 2018). While the degree of impact may vary, both large and small events can cause significant damage due to the immense energy and speed generated during their movement downhill (Nasery et al. 2022; Zhang et al. 2022).

Conducting a rockfall hazard and risk assessment is crucial in minimizing the danger of rockfall incidents in mountainous regions (Koukouvelas et al. 2015; Caviezel et al. 2021). This procedure entails identifying areas where rocks may potentially fall from, evaluating the likelihood and severity of such events, and assessing the potential impact on both human life and infrastructure (Agliardi and Crosta 2003; Tanoli et al. 2022). The most important step for rockfall hazard and risk assessment is rockfall modeling. Rockfall modeling software plays a

crucial role in identifying the patterns of rockfalls in mountainous areas that are critical zones for rockfalls. In general, the use of two-dimensional (2D) and three-dimensional (3D) rockfall modeling software helps in comprehending the dynamics of rockfalls (Schober et al. 2012; Kim et al. 2015). These software have different algorithms and basis (Ansari et al. 2018). Among these models especially 2D models had been used actively, until recently. However, 3D rockfall models, which have emerged with the development of computer technologies, are much more preferred currently (Guzzetti et al. 2002; Lan et al. 2007; Bartelt et al. 2016a; Sellmeier and Thuro 2017; Zhang et al. 2022; Noël et al. 2022). In rockfall studies, 3D models offer great advantages in hazard and risk studies, especially with the use of high-resolution data. For example, simulating the desired number and shape of rock blocks and determining the possible trajectories of the modeled results are some of them (Abellán et al. 2006; Frattini et al. 2013; Kim et al. 2015; Li and Lan 2015; Noël et al. 2022). The most important of these is to observe the rockfall trajectories on 3D surfaces, as well as to solve the hazard and risk problems such as the intersection of the transportation corridors, settlements area, and infrastructure at critical points in a quantitative way (Kim et al. 2015; Dorren and Kühne 2016; Yan et al. 2023).

Rockfall events are a frequently occurring natural disaster in Türkiye, following earthquakes, landslides, and floods (Taga ve Zorlu 2016; Dinçer et al. 2016; Gül et al. 2016; Aydın ve Eker 2017; Geniş et al. 2017; Kayabaşı 2018; Akın et al. 2019b, 2021; Ağca, 2020a, b; Utlu et al. 2021, 2020a, b). Rockfall events generally occur in various locations with different elevations in Türkiye, including transportation corridors, high mountainous areas, and settlements established on high steep slopes. In this study, the hazards associated with rock units with a high potential for falling were evaluated in the Hacıabullah village located in the Central Anatolian region.

Study Area

Hacıabdullah village is located within a valley formed by volcanic rocks on the east slopes of the Melendiz stratovolcano in the Cappadocia region of Türkiye (Figure 1a-c). Generally, rockfall occurring in the Cappadocia region consists of volcanic and volcanic sedimentary units such as andesite-basalt, tuff and ignimbrite (Büyüksaraç et al. 2005; Altın ve Altın 2011; Akın et al. 2019a; Kazancı 2020). Rockfalls are mostly experienced in high-slope areas located north of the Hacıabdullah village (Figure 1d). The inclination of the terrain where rockfall events occur varies between 23 and 90°. In the study area, the steep slope that serves as the source of rockfall events is made up of volcanic rocks with vertical cooling joints, which have been responsible for numerous rockfalls (Figure 2). The study area has semi-arid climate features shown by the letters "BSk" according to the Köppen-Geiger climate classification (Öztürk et al. 2017). Freeze-thaw processes occurring especially during the winter season, gravity on high slope areas, and the general lithology of the study area containing volcanic rocks with heavily jointed structures play dominant roles in triggering rockfall events.

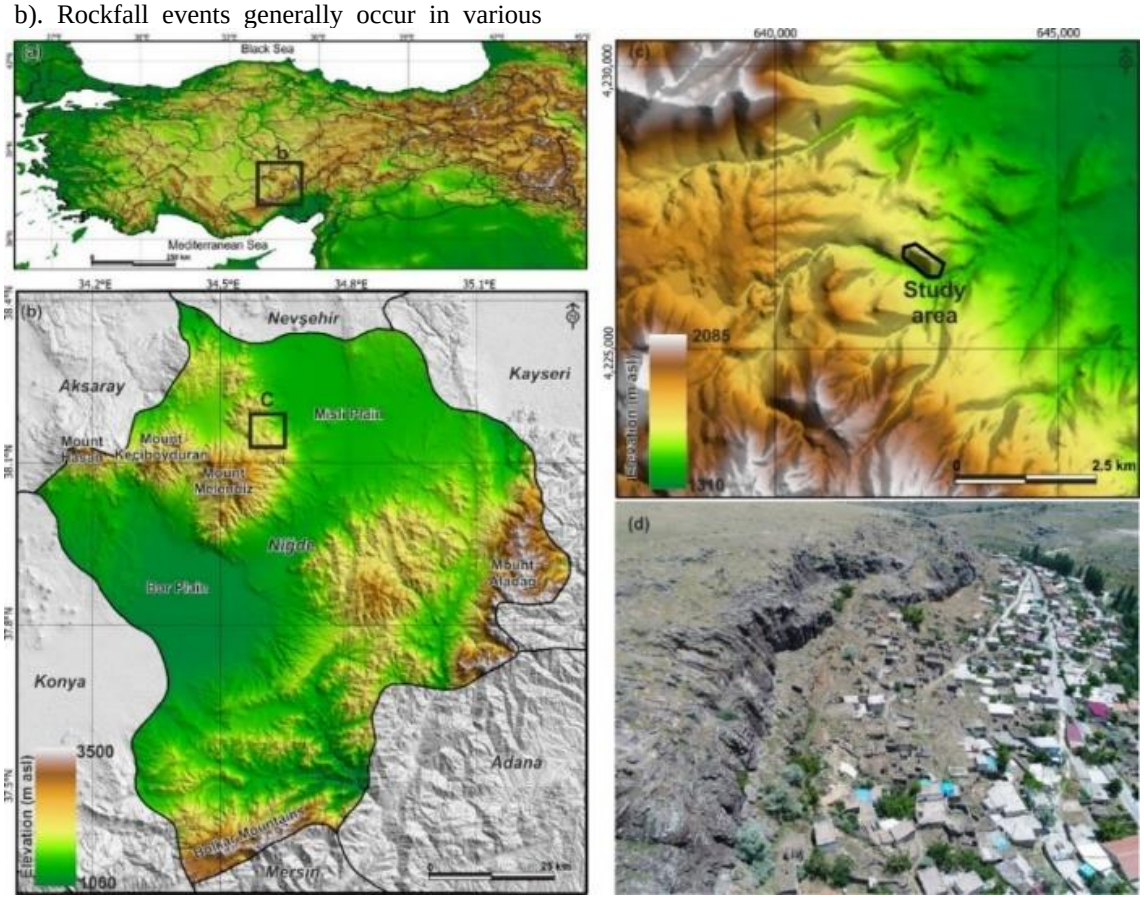

Fig. 1. a-c) Location of the study area and (d) oblique aerial photograph of the study area.

Hacıabdullah village has witnessed several occurrences of rockfall events on different dates since 1957 until now, as reported by the Disaster and Emergency Management Presidency of the Ministry of Interior (AFAD, 2011). AFAD's report documented six significant rockfall incidents that occurred on different dates, including 05/04/1957, 26/06/1963, 13/09/1974, 21/03/1983, 13/11/2007, and 03/03/2008. In the 1957 report, it was recommended to evacuate 85 families who were at risk from rockfalls, but unfortunately, this decision was not followed through by the local community. A report from 1963 also revealed that 92 households suffered damage due to rockfalls and floods. Similarly, in 1974, 12 houses were impacted by rockfalls. The report from 2007 suggested the relocation of 50 houses that were at risk of rockfalls. There are many fallen rocks on the steep slopes of the village and the volumes of these blocks in the area range from 1-19.11 m^3 (Figure 3a-b).

Fig. 2: Cooling cracks and extensions on slopes under rockfall danger

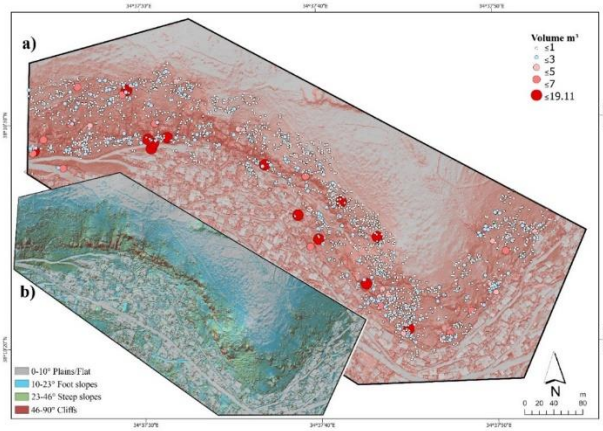

Fig. 3. a) The distributions of the fallen rockfall in the study area and volumes, b) the slope angles (slope descriptions in b were made according to Loye et al. 2009).

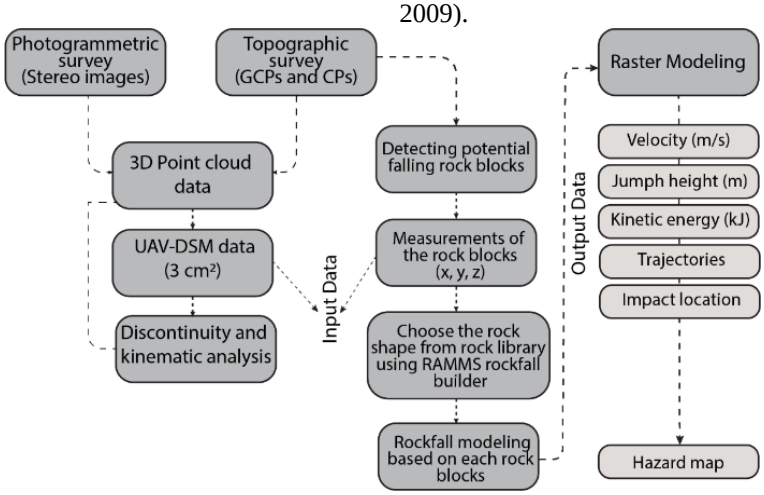

Fig.4. The general flowchart of the study.

Material and methods

Geographic information systems and unmanned aerial vehicle (UAV) technologies were used in the implementation of the study. The GIS-based 3D rockfall program, RAMMS rockfall, was used to model and simulate the hazardous rock blocks identified through field surveys. The trial version of Pix4D was preferred to generate high-resolution UAV-DSM data for the study. The results were mapped using ArcGIS Pro software in the WGS84 UTM 36 Zone projection and coordinate system. The general flowchart for 3D rockfall analysis based on the UAV-DSM and rockfall software is provided in Figure 4. In this scope, a kinematic analysis was conducted along the study area using 3D point cloud data. Additionally, rock blocks with a different volumes and geometry which is potential for falling and hazard were identified throughout the field studies. The geometric properties of these rock blocks were determined as x, y, z. The rock blocks, whose geometric properties and volumes were determined, were simulated according to the high-resolution UAV-DSM data using RAMMS rockfall software. Therefore, the rock blocks hazard potential was determined by identifying their possible trajectories, velocity, jump height, kinetic energy, impact location.

Data acquisition and processing

Accurate analysis is required due to the high hazard and risk status of rockfalls and, from this aspect, modeling studies have great importance (Mary Vick et al. 2019). For rockfall modeling studies, geomorphometric approaches and modeling based on high-resolution DSM data provide more accurate and sensitive results (Loye et al. 2009; Zhang et al. 2019; Pérez-Rey et al. 2019; Francioni et al.

2020; Rodriguez et al. 2020; Akın et al. 2021). Within this scope, UAVs offer significant advantages in producing DSM and orthophoto data for large areas in a short duration and gain great importance for monitoring the distribution of natural disasters, especially, in spatial and temporal terms (Feng and Röshoff 2004; Abellán et al. 2006; Armesto et al. 2009; Alejano et al. 2013; Giordan et al. 2015). High-resolution DSM and orthophoto data are very effective for accurate and sensitive trajectory modeling and the detection of source zones in rockfall-prone areas. For this reason, rockfall studies in recent years have moved beyond traditional methods (Colomina and Molina 2014; Boccardo et al. 2015; Gomez and Purdie 2016; Manconi et al. 2019) and begun to use high-resolution DSM and orthophoto images obtained with UAVs (Matasci et al. 2015; Török et al. 2017; Byrne 2018; Manconi et al. 2019).

UAV Survey and Photogrammetric processing

The development of remote sensing technology and remote sensing platforms such as UAV, Lidar, and Radar technologies allows for obtaining a 3D high-resolution surface/elevation model in a short time. UAV rock mass mapping has emerged as a valuable technology for the detailed and accurate analysis of inaccessible and dangerous rock masses. The use of UAVs equipped with remote sensors allows for the collection of high-resolution images and data of rock masses, which can be used for mapping, monitoring, and analysis (Kasmer et al., 2016, Koukouvelas et al. 2020). In recent years, UAV rock mass mapping has been widely used in geotechnical studies, including rockfall hazard analysis, slope stability analysis, and rock mass characterization (Giordan et al. 2019). The incorporation of UAV-DSM data into rockfall hazard analysis allows for the identification of potential rockfall areas and the determination of the geometry, shape, and size of rock blocks, which are critical parameters for hazard analysis (Corominas et al., 2014). In this study, a DJI Phantom 4 Advanced UAV was used to produce high-resolution orthophoto and digital surface models for rockfall modeling. Technical details and information about the drone model used in the study was given Table 1. The general flowchart followed when producing this data is given in Figure 5.

Table 1: The technical details of the Dji Phantom 4 drones

General		Camera		Battery	
Weight (Battery & Propellers Included)	1380 gr	Sensor	1/2.3 "CMOS	Capacity	5350 mAh
Diagonal Size (Propellers Excluded)	350 mm	Lens	FOV 94° 20 mm	Voltage	15.2 V
Max Ascent Speed	S-mode: 6 m/s	Electronic Shutter Spe	8 - 1/8000 s	Battery type	Lipo 4S
Max Descent Speed	S-mode: 4 m/s	Image Size	4000×3000	Energy	81.3 Wh
Max Flight Time	Approx. 28 minutes			Net weight	462g
Satellite Positioning Systems	GPS/GLONASS			Max charging power	100 W

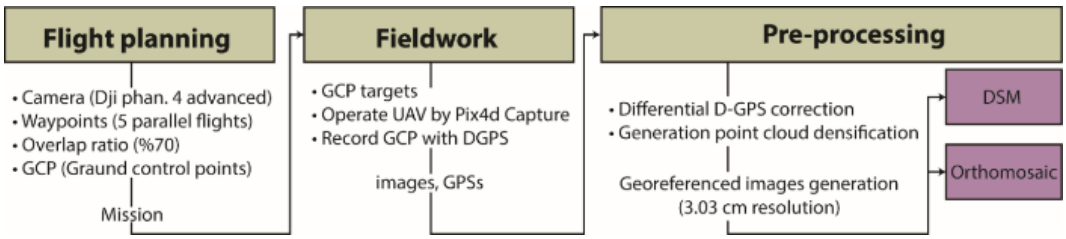

Fig. 5. General flowchart for DSM and orthomosaic generation steps

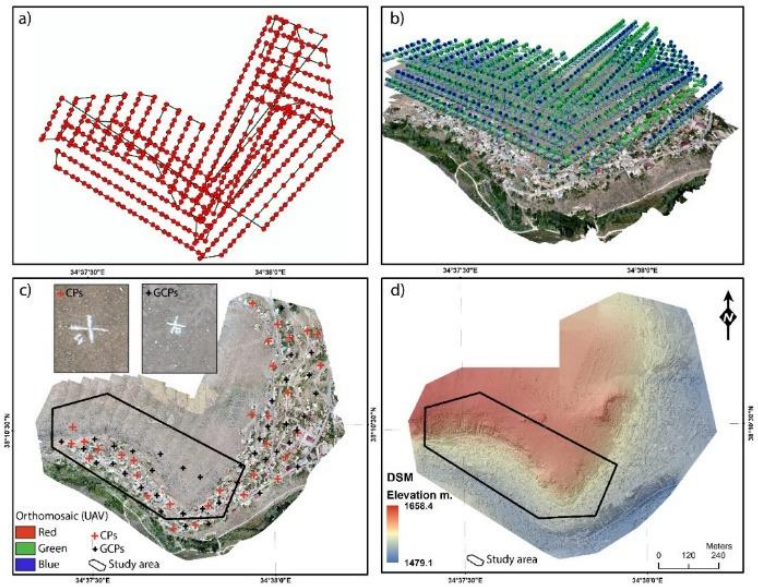

Fig.6. a) The flight paths and location of stereo images, b) location of stereo images on the point cloud, c) The orthomosaic images obtained from photogrammetric processing, d) Digital surface model of the study area (3*3 cm resolution).

Preparations for flight height, scanning width, and stereo image matching proportions were completed with Pix4dcapture software for the study area. To produce DSM and orthophoto data with good quality and sensitivity, 40 ground control points (GCP) were placed with D-GPS before the flight. Five parallel flights were made at 100 meters height, and 621 stereo aerial photographs were obtained with a 70% overlap ratio (Fig. 6a-b). Processing of these images was performed using the Pix4d trial version. Eventually, point cloud data with a 3*3 cm resolution was obtained after the photogrammetric processing of orthophoto images with low (1.4 cm) error (Fig. 6c-d).

Evaluation of the quality of elevation data of DSM

There are some errors when DSM data is obtained using different platforms. These errors are caused by the structure of the land surface and land use/cover features. One of these errors is the vertical error rate (Ajayi et al. 2017; Coveney and Roberts 2017). Ground control points (GCPs) and checkpoints (CPs) are used to fix these errors during collecting stereo images by UAV. To understand the vertical accuracy error rate, CPs data is also collected in addition to the GCPs data. Determining the vertical accuracy rate in DSM data is important for the performance of the study and the precision of the results (Tamminga et al. 2015).

In this respect, using 35 checkpoints in the study area, the vertical accuracy rate of the DSM data root mean square error (RMSE, Formula 1), mean square error (MSE, Formula 2), mean absolute deviation (MAD, Formula3) and mean absolute tested with percentage error (MAPE, Formula 4) (Tamminga et al. 2015; Akturk and Altunel 2019). These formulas are expressed as,

$$\mathrm{RMSE} = \sqrt{\frac{\sum_{t=1}^{n} (A_t - F_t)^2}{n}} \quad \text{(Eq.1)}$$

$$\mathrm{MSE} = \frac{\sum_{t=1}^{n} (A_t - F_t)^2}{n} \quad \text{(Eq.2)}$$

$$\mathrm{MAD} = \frac{\sum_{t=1}^{n} |A_t - F_t|}{n} \quad \text{(Eq.3)}$$

$$\mathrm{MAPE} = \frac{\sum_{t=1}^{n} \left| \frac{A_t - F_t}{A_t} \right|}{n} \times 100 \quad \text{(Eq.4)}$$

The results obtained according to the specified formulas are given in Table 2. Accordingly, the error rates of the DSM data are MAD: 0.169, MSE: 0.066, RMSE: 0.258, MAPE: 0.01 cm Accordingly, DSM data was obtained with a low vertical accuracy error rate.

Table 2: The vertical accuracy results of the DSM data based on different statistical parameters using RMSE, MSE, MAD, MAPE.

Check point	Actual Elevations	Forecast Elevations	Error	Absolute Value of Error	Square of Error	Absolute Values of Errors Divided by Actual Values.
	At	Ft	At -Ft	| At -Ft|	(At -Ft)^2	| (At -Ft)/At|
1	1630.25	1630.10	-0.15	0.150	0.023	0.0001
2	1638.29	1638.13	-0.16	0.160	0.026	0.0001
3	1637.38	1638.00	0.62	0.620	0.384	0.0004
4	1628.94	1628.87	-0.07	0.070	0.005	0.0000
5	1619.62	1619.55	-0.07	0.070	0.005	0.0000
6	1633.70	1632.93	-0.77	0.770	0.593	0.0005
7	1596.07	1595.99	-0.08	0.080	0.006	0.0001
8	1590.10	1590.09	-0.01	0.010	0.000	0.0000
9	1593.89	1593.85	-0.04	0.040	0.002	0.0000
10	1589.94	1589.85	-0.09	0.090	0.008	0.0001
11	1587.47	1588.00	0.53	0.530	0.281	0.0003
12	1593.24	1593.13	-0.11	0.110	0.012	0.0001
13	1631.93	1631.87	-0.06	0.060	0.004	0.0000
14	1569.82	1569.78	-0.04	0.040	0.002	0.0000
15	1612.38	1612.30	-0.08	0.080	0.006	0.0000
16	1566.89	1566.78	-0.11	0.110	0.012	0.0001
17	1622.20	1623.00	0.80	0.800	0.640	0.0005
18	1595.68	1595.60	-0.08	0.080	0.006	0.0001
19	1562.14	1562.00	-0.14	0.140	0.020	0.0001
20	1574.44	1574.32	-0.12	0.120	0.014	0.0001
21	1571.70	1571.60	-0.10	0.100	0.010	0.0001
22	1589.67	1589.60	-0.07	0.070	0.005	0.0000
23	1566.96	1567.10	0.14	0.140	0.020	0.0001
24	1599.51	1599.40	-0.11	0.110	0.012	0.0001
25	1612.30	1612.20	-0.10	0.100	0.010	0.0001
26	1592.02	1591.99	-0.03	0.030	0.001	0.0000
27	1547.38	1547.70	0.32	0.320	0.102	0.0002
28	1556.64	1556.50	-0.14	0.140	0.020	0.0001
29	1586.68	1586.60	-0.08	0.080	0.006	0.0001
30	1576.71	1576.50	-0.21	0.210	0.044	0.0001
31	1583.12	1583.00	-0.12	0.120	0.014	0.0001
32	1553.27	1553.20	-0.07	0.070	0.005	0.0000
33	1548.69	1548.60	-0.09	0.090	0.008	0.0001
34	1555.24	1555.13	-0.11	0.110	0.012	0.0001
35	1552.49	1552.40	-0.09	0.090	0.008	0.0001

Segment detection and measurements

It is crucial to study and comprehend the gaps or cracks within a rock slope because they can significantly impact the stability of the slope and increase the risk of rockfall or mass movements (Xu et al. 2020; Wang et al. 2022). The various kinds of gaps have distinct characteristics that influence the strength and behavior of the rock mass. Factors such as changes in stress levels and weathering can alter the properties of these gaps, making them more or less susceptible to failure. Consequently, having knowledge about the types and properties of gaps within a rock slope is critical to evaluating its stability and identifying potential risks of the blocks (Keskin and Polat 2022).

Discontinuity analysis of rock blocks is a fundamental component of rock mechanics and geotechnical engineering. It involves the systematic examination and characterization of fractures, joints, and other structural weaknesses that occur within the rock mass. This analysis provides valuable information on the strength, stability, and deformation behavior of the rock mass, which are critical factors in engineering design and construction (Monsalve et al. 2021; Wang et al. 2023) and analysis are explained by creating contour diagrams depending on the angle of the extension for the failure patterns of the rock units with the north (Zhang 2006; Riquelme et al. 2018).

In recent years, LIDAR, TLS, and UAV platforms, which are actively used and highly preferred in the creation of digital surface data (DSM-DTM) and play a major role in the creation of discontinuities using point cloud data (Dewez et al. 2016; Riquelme et al. 2017, 2018; Valkaniotis et al. 2018; Monsalve et al. 2021). In this study, 3D point cloud was used for define discontinuous surfaces. The general flowchart is presented in Figure 7.

According to this flowchart, the orientation of slope surfaces causing rockfall in the study area were divided into 3 segments, and the cloud compare software (v2.11.3 version) was used to measure the slope and orientation of each segment using facet/fracture detection plugin. The Facet detection plugin is a custom plugin within CloudCompare v2.6.2 that performs planar facet extraction, calculates slope and aspect directions, and reports the extracted data in interactive stereograms (Dewez et al. 2016). Then, the measurements of the discontinuous surfaces in each segment were performed using the discontinuity set extractor (DSE) (Riquelme et al. 2014). As a result, the slope and orientation of the discontinuous surfaces in each segment were determined (Figure 8).

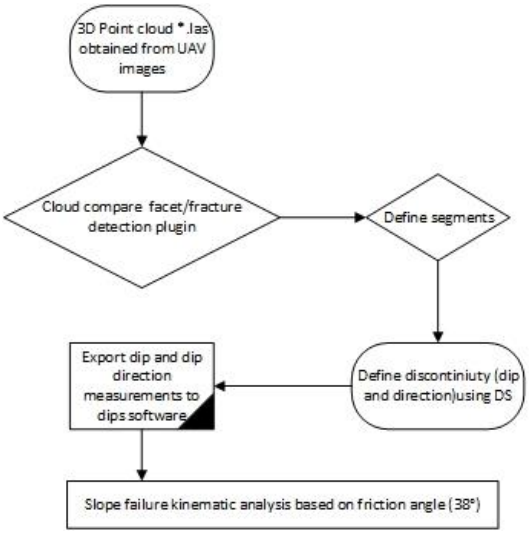

Fig. 7. The general flowchart of the discontinuity and kinematic analysis

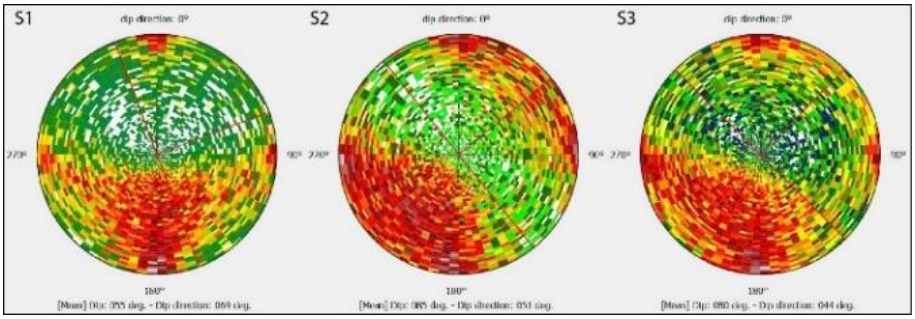

Fig. 8. The overall slope and direction of the segments are as follows: S1. Segment 1., S2: Segment 2. S3: Segment 3.

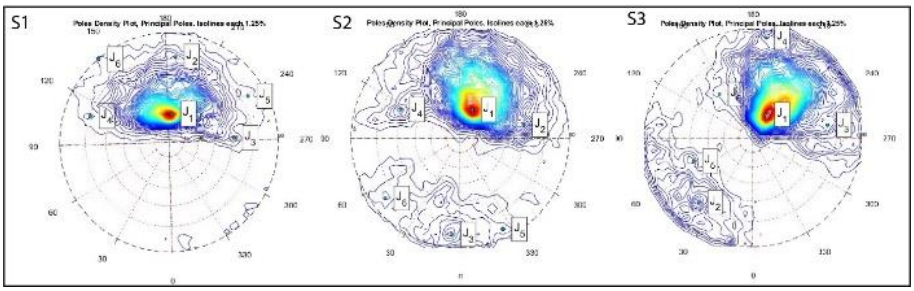

Fig. 9. For each identified segment, the discontinuity sets, slope, and slope direction angles are determined

Discontinuity analysis of the segments using DSE (Discontinuity Set Extractor)

Discontinuity Set Extractor (DSE) is an open-source Matlab-based algorithm developed by Riquelme et al. (2014). It is used to identify, extract, and analyze discontinuities on rock surfaces using a semi-automatic approach. The Discontinuity Set Extractor (DSE) detects the number of discontinuity sets using 3D point clouds. It calculates and analyzes each point on the plane as a separate discontinuity set based on their intervals.

The Facets data obtained for each segment from the CloudCompare software was exported in a .txt file format and transferred to the DSE software. Subsequently, the pole points for the slope and direction of the

discontinuities in the segments were obtained. These pole points were edited to identify the principal sets of discontinuities with the highest density (Figure 9) based on discontinuity sets belonging segments (Table 3).

Table 3. High-density discontinuity sets belonging to segments.

Segments	Joint Count	Dip/ Dip direction
S1	6 (J_1,J_2,J_3,J_4,J_5,J_6)	29/187-76/185-61/267-74/190-79/241-89/141
S2	6 (J_1,J_2,J_3,J_4,J_5,J_6)	31/202-61/258-82/4-62/115-85/334-82/51
S3	6 (J_1,J_2,J_3,J_4,J_5, J_6)	27/209-75/40-69/260-86/187-60/68-53/142

Kinematic analysis

The dominant discontinuity sets and kinematic analyses were carried out by transferring the values of dip and dip direction to the Dips v.7.0 (Rocscience 2016) software environment. During the kinematic analysis, the internal friction angle value was taken as an average of 38°. The internal friction coefficient, which shows variation between maximum and minimum values, was determined based on previous studies conducted on Melendiz Volcanics and surrounding tuff, ignimbrite, and andesite units (Acar 2011; Akın et al. 2019a), and applied in the current study.

As a result, it was observed that these surfaces, which were subjected to kinematic analyses, have a different discontinuity surface and widely spaced joints on each segment. (Figure 10). According to the kinematic analysis results, while toppling-type failures occur along Segment 1, both wedge and toppling failures occur along Segment 2, with both having a very low probability of around 13%. Along Segment 3, it is observed that wedge-type failures with a potential of approximately 46% occur due to the intersection of discontinuities. Furthermore, out of the 6 discontinuity sets along Segment 3, 2 of them have a potential for both toppling and planar sliding, with a probability of 33%. Kinematically, wedge and toppling failures are more prevalent, while planar sliding is observed in a limited number of slopes. Rock mass instabilities that begin with planar sliding, wedging, and toppling continue as falling and rolling of rock masses depending on the general slope inclination. This can potentially cause damage to residential areas.

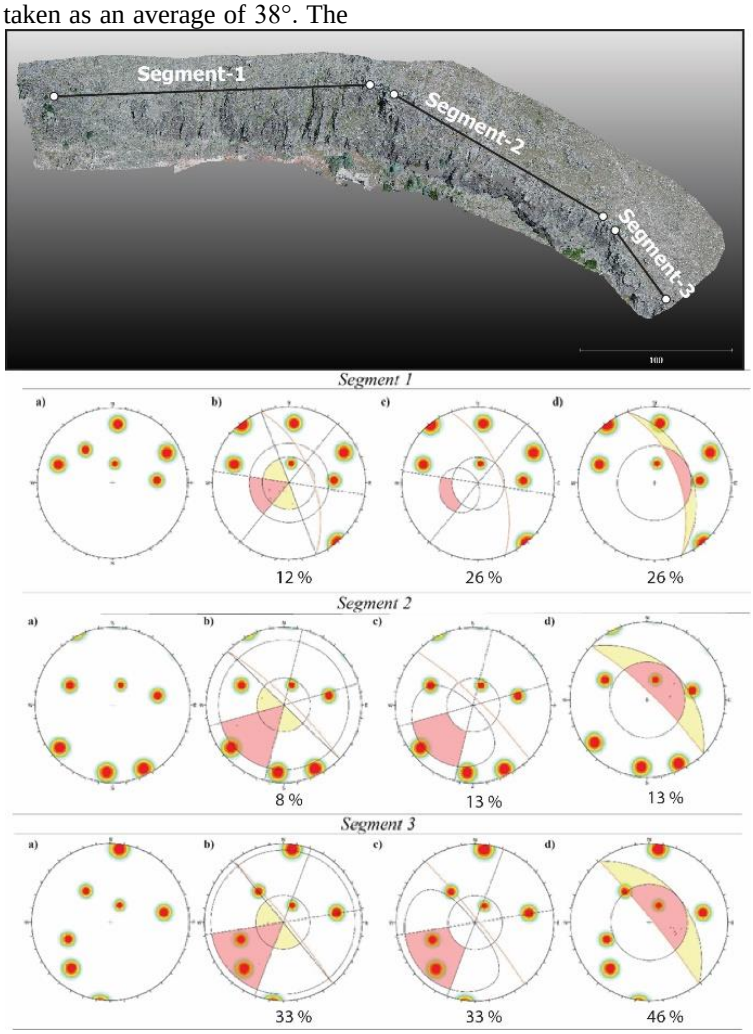

Fig. 10. a) For each segment, and characteristics of the discontinuity sets, including b) planar sliding, c) wedge failure, and d) toppling failure.

Block geometries

To identify blocks that have potential falling risks, field studies were performed and 17 blocks were identified (Figure 11). The height, width, and length were measured for each block and according to these values each rock is modeled in 3D RAMMS: ROCKFALL 1.6. 70 module Software. The rock density of the rock block on the RAMMS rockfall library is 2700kg/m3 as standard. Accordingly, 17 risky rock blocks have a density between 2943-32400 kg (Table 4). While 10 of the modeled rock blocks (R1-R2-R4-R6-R7-R10-R11-R15-R16-R17) have equant and real-equant geometry, 5 rocks (R3-R9-R12-R13-R14) have long and real-long geometry and R5-R8 blocks have flat geometry (Figure 12).

Table 4. Properties of the simulated rocks

No	X	Y	Z	Vol (m^3)	Mass density (Kg)	Rock shape
R1	3.2	2.5	1.5	12	32400	Equant
R2	2.0	1.8	1.0	3.6	9720	Equant
R3	1.5	1.6	1.2	5.03	13581	Real long
R4	1.42	1.23	1.0	1.74	4698	Real Equant
R5	1.2	1.4	0.8	1.34	3618	Real Flat
R6	1.5	1.25	1.0	1.87	5049	Equant
R7	1.5	1.25	1.0	1.87	5049	Equant
R8	1.22	1.17	1.0	1.42	3834	Real Flat
R9	0.96	1.16	0.98	1.09	2943	Real Long
R10	1.42	1.23	1.0	1.74	4698	Real Equant
R11	1.42	1.23	1.0	1.74	4698	Real Equant
R12	1.15	1.49	1.0	1.71	4617	Real Long
R13	3.24	1.62	2.23	11.7	31590	Real Long
R14	1.56	2.01	1.35	4.23	11421	Real Long
R15	1.42	1.23	1.0	1.74	4698	Real Equant
R16	1.61	1.34	1.07	2.3	6210	Equant
R17	2.18	2.34	1.87	9.53	25731	Real Equant

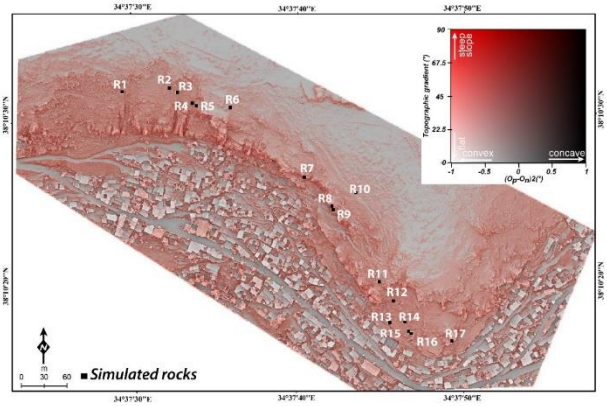

Fig. 11. Red Relief Image Map (RRIM) of the study area and distribution of rock blocks have high fall risk

RAMMS software provides a great advantage for accurate and high-quality modeling of rocks with different shapes and volumes measured in field studies (Mary Vick et al. 2019) and takes into account the real size of blocks (Dorren and Kühne 2016; Torsello et al. 2021). The Red Relief Images (RRIM) map was used to visualize and interpret the analysis results. (Figure 11). RRIMs can be useful for visualizing positive (O_p) and negative openness (O_n) because they allow for easy identification of high and low-elevation areas. High-elevation areas that are surrounded by lower-elevation areas (i.e., peaks or ridges) would appear as red areas in a RRIM and In contrast, low-elevation areas that are surrounded by higher-elevation areas (i.e., valleys or depressions) (Chiba et al. 2008, 2019).

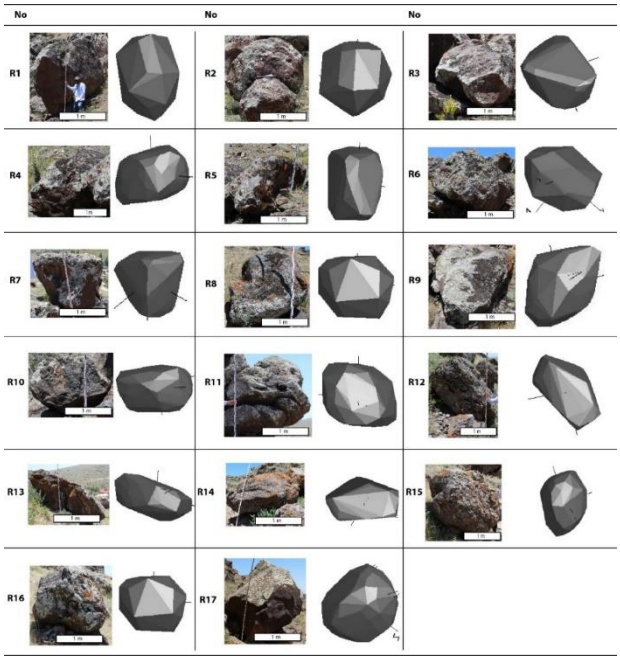

Fig. 12: Photographs of rocks identified in field studies and model forms of these rocks in the RAMMS

Rockfall simulations

Several rockfall models have been created to evaluate various factors related to rockfalls such as dynamics, trajectories, kinetic energy, velocity, jump height, and more (Azzoni et al. 1995; Dorren 2003; Volkwein et al. 2011; Frattini et al. 2012; Žabota et al. 2021; Liu et al. 2021). RAMMS, CONEFALL, STONE, Georock, Rockyfor3D, FlowR, and Rotomap produce two-dimensional (2D) and 3D rockfall models based on different algorithms and GIS for spatial analysis (Wieczorek et al. 1998; Guzzetti et al. 2002; Jaboyedoff and Labiouse 2011; Topal et al. 2012; Bartelt et al. 2016a; Zhang et al. 2022). 3D rockfall simulations are performed on 3D surface/elevation models to determine rockfall trajectories and runout zones (Dorren 2003). The results obtained from these models offer advantages in creating hazard maps for various rockfall-related parameters such as susceptibility, vulnerability, protection, occurrence, and distribution (Vo 2015; Bonneau et al. 2018; Sarro et al. 2018; Singh et al. 2018; Sazid 2019).

In this study, after determining the geometric and volumetric properties of these blocks with very different shapes and volumes, 3D rockfall analyses were executed with the RAMMS: Rockfall software which is a GIS-based 3D rockfall simulation program (Leine et al. 2014; Bartelt et al. 2016a). RAMMS software enables the modeling of rock blocks in different shapes and geometries in the source zones with the potential to fall or with the potential of serious danger and risk. Accordingly, RAMMS software plays an important role as it provides a more realistic simulation of rock blocks and shapes compared to other rockfall software. Thus, in comparison

to many other software programs, the RAMMS rockfall module offers a more sophisticated and realistic approach to rockfall simulation, allowing for the consideration of a variety of factors that can affect the motion of falling rocks and boulders. To conduct rockfall modeling, a variety of data inputs are necessary, along with the modeling data obtained through DSM (Digital Surface Model) data. These inputs include characteristics like plant cover (open, dense, etc.), terrain types (hard, extra hard, medium, soft, medium soft, etc.), and block types (flat, equitant, round, etc.) for blocks or source zone areas to be modeled by the RAMMS program (Vo 2015). The categorization of terrain into specific types such as "hard", "extra hard", "medium", "soft", or "medium-soft" typically refers to the geological and geotechnical characteristics of the terrain. According to their durability and resistance to deformation, these characteristics are frequently used to categorize the soil or rock mass. For instance, "hard" terrain typically refers to solid and long-lasting rock formations like granite or basalt. Since they have a high compressive strength and a slow rate of deformation, these kinds of rock formations are resistant to weathering and erosion. The term "soft" terrain typically refers to soils or rock formations that are relatively weak and deformable, like clay or sandstone. Because of their lower compressive strength and higher deformation rates, these formations are more prone to rockfalls. For rockfall modeling in the RAMMS program, DSM data with a resolution from 1-10 m is sufficient. For this reason, DSM data with cm resolution was rescaled to the 1-meter resolution to obtain the format for use in modeling. Because the advantage of rescaling to a lower resolution is that it reduces the file size and makes the data easier to process and analyze. Considering the volcanic rocks in the field, the terrain type was selected as hard terrain, covered with very sparse plant cover (Figure 1d). Besides, the friction parameters (Table 5) were determined based on terrain type that accounts for; “Rocks jump over the ground, includes different size of blocks and absence of the vegetation” (Bartelt et al. 2016b).

Table 5. The friction parameters of the simulated rockfalls (Bartelt et al. 2016b).

Material strength		**Material weakening**	**Rock ejection**	**Material behavior**
μ min	μ min	β	κ	v
0.55	2	185	3	0.4

Rockfall Hazard Index

The Rockfall Hazard Index (RHI) is a quantitative method used to evaluate the potential rockfall hazard in a given area. It was introduced by Crosta and Agliardi in 2003 and is based on the analysis of the interaction between the rock slope and the rockfall trajectories. The RHI is a dimensionless index that ranges from 0 to 1, where 0 represents no hazard and 1 represents the highest hazard (Crosta and Agliardi 2003). This method involves the following steps: I) Identification of rockfall source areas, II) calculation of the runout distance, III) calculation of the kinetic energy, IV) calculation of the probability of impact, V) calculation of the RHI (RHI is calculated by multiplying the kinetic energy by the probability of impact and normalizing the result by the maximum possible value) that all parameters are taken into consideration which was determined through the RAMMS program in this study. Necessary classifications for kinetic energy, jump height, and block count values are presented in Table 6. For the calculation of block count value, the c/(5*n) formula was used and then reclassification was performed (Crosta and Agliardi 2003). The block count method is a qualitative method used to assess rockfall hazards. It involves counting the number of potentially unstable blocks on a rock slope and categorizing them according to their size and potential energy. This method is based on the assumption that the more unstable blocks there are on a slope, the higher the rockfall hazard. As we can see in the formula, c represents rockfall count, and n represents the number of blocks from each cell value. The values obtained as a result of the modeling of the rock blocks were evaluated separately for each block based on RHI. The values obtained were separately calculated to reach the rockfall model with the results of the classification of the 3 parameters combined to identify high-moderate-low hazard areas.

Table 6. Classification of parameters according to the Rockfall Hazard Index method (Crosta and Agliardi, 2003).

Class	Block count (local scale)	Kinetic energy (kJ)	Jump height (m)
1	< 0.01	≤ 700	≤ 4
2	0.01 – 0.1	700 – 2500	4 – 10
3	> 0.1	≥ 2500	≥ 10

Results

The 17 rock blocks identified have varying geometric properties and volumes, with heights ranging from 0.8 to 2.23 m, lengths from 0.96 to 3.2 m, and widths of 1.16 to 2.5 m. (Figure 12). As a result of these dimensions, the volume of blocks was calculated between 1.09 and 12 m^3, while block mass was calculated to be in a range of 2943-32400 kg The block shapes were identified as equant, real long, real equant, and real flat in the RAMMS program based on measurements in the fields. A total of 100 throws for each block at 17 different release locations were modelled and the kinetic energy (kJ), velocity (m/s), jump height (m), impact location, trajectoris and Rockfall Hazard Index were determined. As a result of the shape and volume of the blocks, as well as the slope features, rocks display differences in their runout distances. Just as the geometric shapes of blocks and topographic profiles of the area affect the kinetic energy, they also control the block velocity and the jump height. Generally, high velocity and jump height values are obtained at the areas where kinetic energy reaches maximum levels. Model results showed maximum kinetic energy values (3476.8 kJ), seeing that on equant geometry of blocks, while low kinetic energy values (90.6 kJ) seeing that on flat and long geometry of blocks (Figure 13). With 90.6 kJ, the lowest value is found in R5 with a flat geometry, while the highest value is found in R1 with equant geometry. The rock velocity values vary depending on the topography of

the field and the slope. The velocity values between 8 and 23.1 m/s reach. The maximum and minimum velocities were observed in R11 and R13, respectively. In addition to these values, while equant-shaped rock blocks exhibit a velocity value between 10-23.1 m/s, flat and long blocks show a velocity value between 8.74 and 19.93 m/s. Jump height values range between 1.99 and 14.5 m. Equant blocks have values ranging from 3.4-14.5 m, while long and flat blocks have values between 1.99 and 7.8 m. As seen for blocks R1, R4, R6, R7, R8, R9, R10, R11, R12, R14, R15, R16, and R17 represent equant features that involve different sizes and volumes present different run-out distances based on the geometry of the blocks. Apart from this, the R12 block has a continuous slope profile; however, the block could not progress a long distance due to the different shape (real long). A rock block with equant geometry has a runout distance of 53.1-126.9 m, whereas a flat or long geometry has a runout distance of 34-122.9 m. In the case of the rock block R8, whose value is 122.9 m, the trajectory was carried over long distances due to the continuous steep slopes (Figure 13).

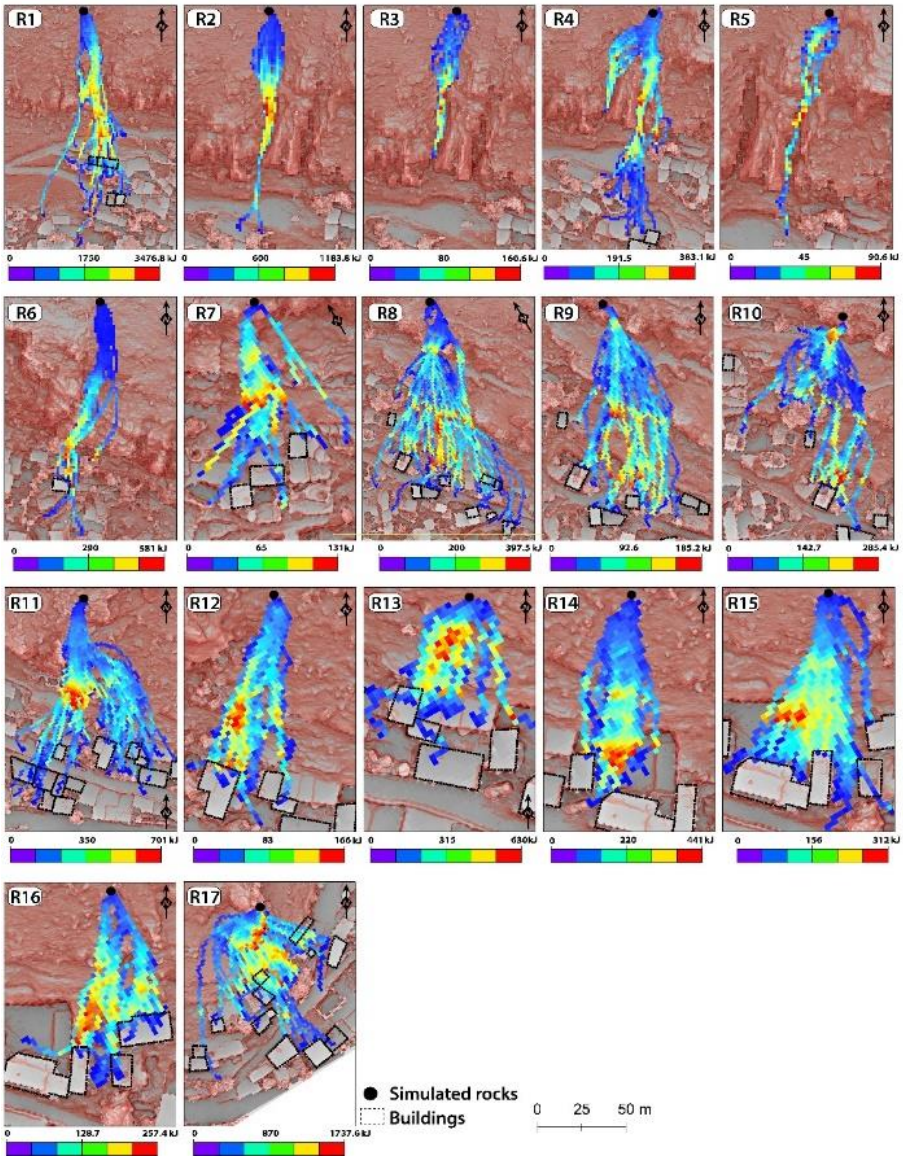

Fig. 13. Rockfall trajectories and kinetic energy values of 17 blocks

The block with the lowest kinetic energy, jump height, and velocity value appeared to be block number R5 with a flat geometry (Table 7). The jump height values obtained by rockfall modeling indicate that the blocks may jump over the settlement units under suitable topographic conditions and cover long distances damaging houses and walls. As can be seen from the modeling results, while a total of 11 blocks exceeds the houses (R1-R7-R8-R9-R10-R11-R12-R13-R15-R16-R17), only 6 blocks (R2-R3-R4-R5-R6-R14) are damped before reaching the houses due to their low kinetic energy and jump height values.

Rockfall Hazard Assessment

The rockfall trajectories determined using rockfall simulations point out a significant risk for the investigated settlement and summarized in Table 7. Blocks falling from vertical steep slopes generally stop on the roads before reaching the settlement units. However, apart from R2, R3, and R5, a total of 14 different blocks may damage

residential units in the study area. These blocks have very high risk due to being transported over long distances. It appears they may cause great damage and even loss of life due to high energy, velocity, and jump height.

Table 7: Rockfall parameters obtained by 3D rockfall modeling (H: House, T: Tree, R: Road)

No	Max. kinetic energy (kJ)	Max. velocity (m/s)	Max. jump height (m)	Max. runout distance (m)	Element at risk
R1	3476.8	16.73	5.25	126.9	H,T,R
R2	1183.5	14.53	4.25	81.6	T,R
R3	160.6	10.15	2.27	59.8	T,R
R4	383.1	16.46	5.75	112.5	H,T,R
R5	90.6	8.17	1.99	75.8	No contact
R6	581	17.9	9.02	94	H,T
R7	131	17.19	8.71	55.07	Abandoned H
R8	397.5	19.93	7.83	122.9	H,T,R
R9	185.2	16.51	6.84	85.2	H,T,R
R10	285.4	13.71	6.05	84	H,T,R
R11	701	23.1	14.57	90.1	H,T,R
R12	166	12.06	4.1	56.6	H,T
R13	630	8.74	4.55	34.5	H
R14	441	13	6.23	44.8	H
R15	312	14.63	6.42	65.3	H,T,R
R16	257.4	10.61	3.04	53.1	H,T
R17	1737.6	16.05	10.1	69.7	H,T,R

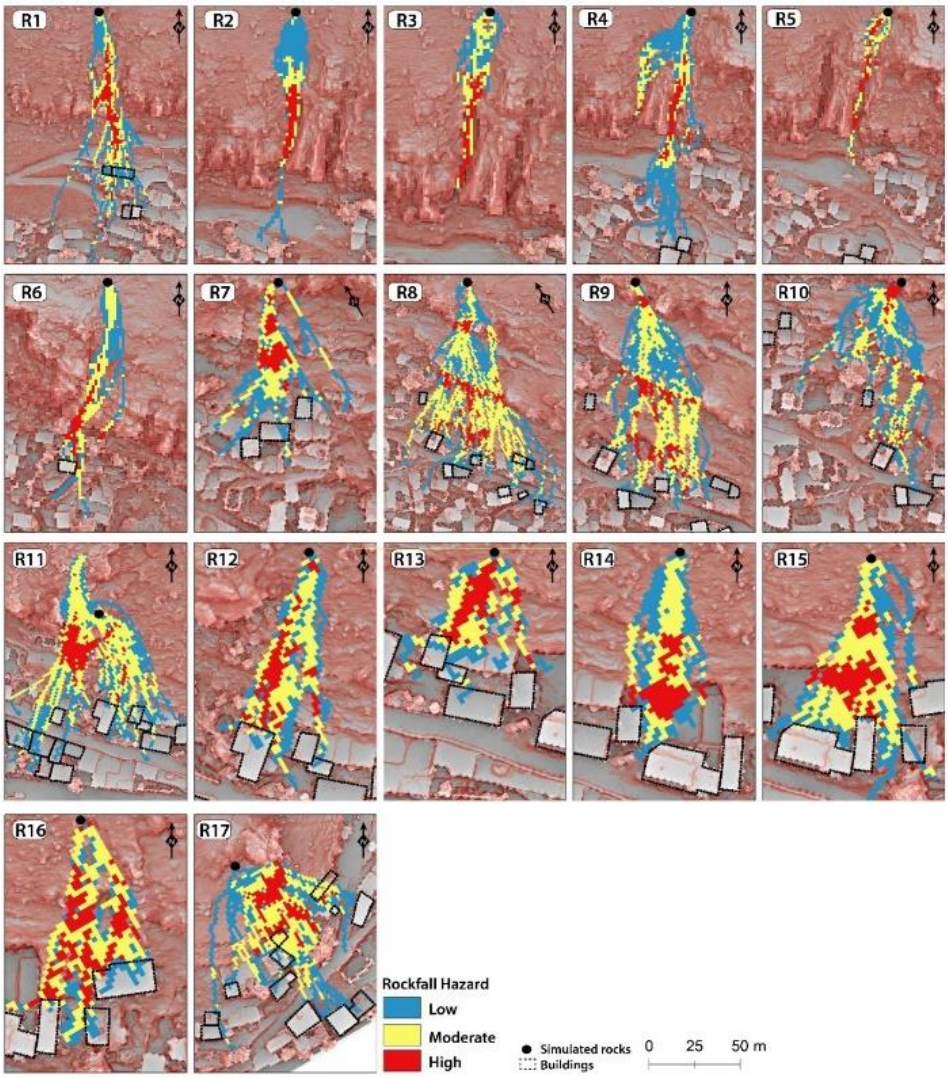

Fig. 14. Rockfall Hazard Index results of the rock blocks.

According to the hazard map, modeling of rocks R6, R12, R13, R14, R15, R16, and R17 indicates that settlement areas constitute most of the high and moderate-risk areas.

According to the hazard map, modeling of rocks R6, R12, R13, R14, R15, R16, and R17 indicates that settlement areas constitute most of the high and moderate-risk areas.

Conclusions

Unmanned Aerial Vehicle (UAVs) is an important data collection platform for remote sensing technologies, especially for mass movements and rockfalls in terms of natural disasters. Particularly, providing detailed and up-to-date topographic datasets is important for the high precision and accuracy of 3D modeling. Identifying the rock blocks that are difficult to detect in terms of source zones and movement stability is critical for preventing rockfalls or reducing potential damages, and the results obtained are of great importance. Therefore, the use of UAV platforms is crucial for understanding the dynamics of rockfall events.

In this study, rockfall events that occur intensively in Haciabullah village were investigated. High-resolution UAV-DSM data were used to examine the rockfall hazards. Within this scope, rock blocks with falling potential that put the village in danger were identified with the support of fieldwork. As a result of the identification of 17 different rock blocks, these blocks were modeled using the 3D Rockfall simulations program, RAMMS. In the simulation study, each rock block was simulated 100 times, and important findings were made through modeling. Based on RAMMS analysis, the kinetic energy varies between 90.6 and 3476 kJ, the velocity between 8.17 and 23.1 m/s, and the jump height between 1.99 and 14.57 meters. These values show variation according to the general slope values for the study area and trajectory of the modeled blocks the slope profile and geomorphology of the study area, and the geometry and volume of the blocks. Rock blocks may travel very long distances in regions with slope values below 46°, while blocks stop on slope breaks without traveling long distances when slope values are from 46-90°. Some of the results of rockfalls modeling show the trajectories that channeled into valleys ended within the valley, while some of the results of rockfalls found on ridges show large areas are threatened. As a result of the shape and volume of the blocks, as well as the slope features, rocks display differences in their runout distances after falls. A rock block with equant geometry has a runout distance of 53.1-126.9 m, whereas a flat or long geometry has a runout distance of 34-122.9 m. It should be noted that the residential houses are mostly demolished and thus some trajectories are rolling over the remnants of these buildings. According to the hazard map, R6, R12, R13, R14, R15, R16, and R17 involve high and moderate levels of risk for settlement units. R1, R4, R7, R8, R9, and R10 show that the majority of them involve low risk, while a small portion is a moderate risk. Taking the necessary precautions for the determined risk areas has vital importance due to the frequent experience of rockfalls in the area. The model outcomes should be considered when taking the necessary precautions. In conclusion, in Hacıabdullah village where rockfall events are actively experienced, the risk for settlement areas and the spatial distribution of the possible risk were accurately revealed by field study results and rockfall models completed with a high-resolution digital elevation model produced with the aid of a UAV. These results have great importance in terms of taking the necessary precautions based on rockfall hazard maps.

Acknowledgements

The authors thank Dr. Mutluhan Akin for providing for valuable discussions and inspiration. We want to thank all participants of the of the article. We also thank the referees and editors for their constructive feedback regarding the initial version of the manuscript.

Authors Contributions

Conceptualization, M.U and M.Z.Ö.; methodology, M.U and M.Z.Ö.; software, M.U.; validation, M.F.A.- M.Ş.; formal analysis, M.U.-M.Z.Ö. and M.Ş.; investigation, M.Z.Ö. and M.Ş; resources, M.U., M.Z.Ö. and M.Ş.; data curation, M.U.; writing—original draft preparation, M.U.; writing—review and editing, M.U., M.Z.Ö., M.Ş and M.F.A.; visualization, M.U. All authors read and agreed to the published version of the manuscript.

References

Abellán A, Vilaplana JM, Martínez J (2006). Application of a long-range Terrestrial Laser Scanner to a detailed rockfall study at Vall de Núria (Eastern Pyrenees, Spain). *Int J Rock Mech Min Sci Geomech* 88:136–148. DOI:10.1016/j.enggeo.2006.09.012

AFAD (2011). Hacıabdullah Jeolojik Etüd Raporu. T.C. Niğde Valiliği, İl Afet ve Acil Durum Müdürlüğü., 23pp"

Agliardi F, Crosta GB (2003). High resolution three-dimensional numerical modelling of rockfalls. *Int J Rock Mech Min Sci* 40:455–471.

Ağca, M., Kaya, E., Yılmaz, HM (2020a). Yersel ve fotogrametrik yöntemler ile kaya bloklarının hacimlerinin hesaplanması: Selime örneği, Aksaray. *Afyon Kocatepe Üniversitesi Fen Ve Mühendislik Bilimleri Dergisi,* 20(3), 465-471.

Ağca, M., Gültekin, N.Y., Kaya, E (2020b). İnsansız hava aracından elde edilen veriler ile kaya düşme potansiyelinin değerlendirilmesi: Adam Kayalar örneği, Mersin. *Geomatik*, 5(2), 134-145.

Ajayi OG, Salubi AA, Angbas AF, Odigure MG (2017). Generation of accurate digital elevation models from UAV acquired low percentage overlapping images. *Int. J. Remote Sens.* 38:3113–3134.

Akın M, Dinçer İ, Ok A.Ö, et al (2021). Assessment of the effectiveness of a rockfall ditch through 3-D probabilistic rockfall simulations and automated image processing. *Eng Geol* 283:106001. DOI:10.1016/j.enggeo.2021.106001.

Akın M, Dinçer I, Orhan A, et al (2019a). Kaya Tutma Hendek Performansının 3-Boyutlu Kaya Düşme Analizleriyle Değerlendirilmesi: Akköy (Ürgüp) Örneği. *Jeol Mühendisliği Derg* 211–231. DOI:10.24232/jmd.655005.

Akın M, Dinçer İ, Orhan A, et al (2019b). Evaluation of the Performance of a Rockfall Ditch by 3-Dimensional Rockfall Analyses: Akköy (Ürgüp) Case. *Jeol Muhendisligi Derg* 43:211–232. DOI:10. 24232/jmd.655005.

Akturk E, Altunel AO (2019). Accuracy assessment of a low-cost UAV derived digital elevation model (DEM) in a highly broken and vegetated terrain. *Measurement* 136:382–386. DOI:10.1016/j.measurement.2018.12.101

Alejano LR, García-Cortés S, García-Bastante F, Martínez-Alegría R (2013). Study of a rockfall in a limy conglomerate canyon (Covarrubias, Burgos, N. Spain). *Environ Earth Sci* 70:2703–2717. DOI:10.1007/s12665-013-2327-x.

Altın TB, Altın BN (2011). Development and morphometry of drainage network in volcanic terrain, Central Anatolia, Turkey. *Geomorphology* 125:485–503. DOI:10.1016/j.geomorph.2010.09.023.

Ansari MK, Ahmad M, Singh R, Singh TN (2018). 2D and 3D rockfall hazard analysis and protection measures for Saptashrungi Gad Temple, Vani, Nashik, Maharashtra – A case study. *J Geol Soc India* 91:47–56. DOI:10.1007/s12594-018-0819-8

Armesto J, Ordóñez C, Alejano L, Arias P (2009). Terrestrial laser scanning used to determine the geometry of a granite boulder for stability analysis purposes. *Geomorphology* 106:271–277. DOI:10. 1016/j.geomorph.2008.11.005

Aydın A, Eker R (2017). Kaya yuvarlanmalarından etkilenen orman alanlarının belirlenmesi: İnebolu örneği. *İstanbul Üniversitesi Orman Fakültesi Derg* 67:136–149. DOI:10.17099/jffiu.28171

Azzoni A, La Barbera G, Zaninetti A (1995). Analysis and prediction of rockfalls using a mathematical model. *Int J Rock Mech Min Sci* 32:709–724. DOI:10.1016/0148-9062(95)00018-C.

Baillifard F, Jaboyedoff M, Sartori M (2010). Rockfall hazard mapping along a mountainous road in Switzerland using a GIS-based parameter rating approach. *Nat Hazards Earth Syst Sc*i 3:435–442. DOI:10.5194/nhess-3-435-2003.

Bartelt P, Bieler C, Bühler Y, et al (2016a). RAMMS::ROCKFALL User Manual v1.6. 102

Bartelt P, Gerber W, Christen M, Bühler Y (2016b) Modeling rockfall trajectories with non-smooth contact/impact mechanics. Içinde: *13th Congress Interpraevent 2016.* 203–211

Berger F, Rey F (2004). Mountain protection forests against natural hazards and risks: New french developments by integrating forests in risk zoning. *Nat Hazards* 33:395–404. DOI:10.1023/B:NHAZ. 0000048468.67886.e5

Boccardo P, Chiabrando F, Dutto F, et al (2015). UAV Deployment Exercise for Mapping Purposes: Evaluation of Emergency Response Applications. *Sensors* 15:15717–15737. DOI:10.3390/s150715717

Bonneau DA, Hutchinson DJ, Difrancesco P, et al (2018) 3-Dimensional Rockfall Shape Back-Analysis : Methods and Implications. 1–35. DOI:10.5194/nhess-2018-366

Büyüksaraç A, Jordanova D, Ateş A, Karloukovski V (2005) Kapadokya İgnimbiritleri ve Volkanitlerinde Paleomanyetik Çalışma-Manyetik Anomalilerin Yorumuna Bir Yaklaşım. *İstanbul Üniv Müh Fak Yerbilim Derg* 18:199–218

Byrne K (2018) Digital Morphometry Applied to Geo-Hazard Risk Assessment: A Case Study from Germany. Technische Universitat Dresden, Faculty of Environmental Sciences, Institute for Cartography, Master of Science

Caviezel A, Ringenbach A, Demmel SE, et al (2021) The relevance of rock shape over mass—implications for rockfall hazard assessments. *Nat Commun* 12:1–9. DOI:10.1038/s41467-021-25794-y

Chiba T, Kaneta S, Ohashi M (2019) Digital Terrain Representation Methods and Red Relief Image Map, *A New Visualization Approach. Proc ICA* 2:1–3. DOI:10.5194/ica-proc-2-17-2019

Chiba T, Kaneta S, Suzuki Y (2008) Red relief image map: New visualization method for three dimensional data. *Int Arch Photogramm Remote Sens Spat Inf Sci* 37:1071–1076. DOI:10.11212/jjca1963.45.27

Colomina I, Molina P (2014) Unmanned aerial systems for photogrammetry and remote sensing: A review. *ISPRS J Photogramm Remote Sens* 92:79–97. DOI:10.1016/j.isprsjprs.2014.02.013

Corominas, J., van Westen, C., Frattini, P. et al. (2014). Recommendations for the quantitative analysis of landslide risk. *Bull Eng Geol Environ 7*3, 209–263 . https://doi.org/10.1007/s10064-013-0538-8

Coveney S, Roberts K (2017) Lightweight UAV digital elevation models and orthoimagery for environmental applications: data accuracy evaluation and potential for river flood risk modelling. *Int J Remote Sens* 38:3159–3180. DOI:10.1080/01431161.2017. 1292074

Crosta GB, Agliardi F (2003) A methodology for physically based rockfall hazard assessment. *Nat Hazards Earth Syst Sci* 3:407–422. DOI:10.5194/nhess-3-407-2003

Dewez TJB, Girardeau-Montaut D, Allanic C, Rohmer J (2016) Facets : A cloudcompare plugin to extract geological planes from unstructured 3d point clouds. Int. Arch. Photogramm. *Remote Sens. Spat. Inf. Sci.* - ISPRS Arch. 41:799–804

Dinçer İ, Orhan A, Frattini P, Crosta GB (2016) Rockfall at the heritage site of the Tatlarin Underground City (Cappadocia, Turkey). *Nat Hazards* 82:1075–1098. DOI:10.1007/s11069-016-2234-z

Dorren L, Kühne R (2016) Comparing the 3D rockfall simulation models Rockyfor3D and RAMMS :: ROCKFALL at a case study site in Switzerland. *INTERPRAEVENT* 2016 – Ext. Abstr. 2–3

Dorren LKA (2003) A review of rockfall mechanics and modelling approaches. *Prog Phys Geogr* 27:69–87. DOI:10.1191/0309133303pp359ra

Dorren LKA, Maier B, Putters US, Seijmonsbergen AC (2004) Combining field and modelling techniques to assess rockfall dynamics on a protection forest hillslope in the European Alps. *Geomorphology* 57:151–167. DOI:10.1016/S0169-555X(03)00100-4

Dorren LKA, Seijmonsbergen AC (2003) Comparison of three GIS-based models for predicting rockfall runout zones at a regional scale. *Geomorphology* 56:49–64. DOI:10.1016/S0169-555X(03)00045-X

Fanos AM, Pradhan B (2018) Laser Scanning Systems and Techniques in Rockfall Source Identification and Risk Assessment: A Critical Review. *Earth Syst Environ* 2:163–182. DOI:10.1007/s41748-018-0046-x

Farvacque M, Lopez-Saez J, Corona C, et al (2019) Quantitative risk assessment in a rockfall-prone area: the case study of the Crolles municipality (Massif de la Chartreuse, French Alps). *Géomorphologie Reli Process Environ* 25:7–19. DOI:10.4000/geomorphologie.12778

Feng L, Intrieri E, Pazzi V, et al (2021) A framework for temporal and spatial rockfall early warning using micro-seismic monitoring. *Landslides* 18:1059–1070. DOI:10.1007/s10346-020-01534-z

Feng QH, Röshoff K (2004) In-situ mapping and documentation of rock faces using a full-coverage 3d laser scanning technique. *Int J Rock Mech Min Sci* 41:1–6. DOI:10.1016/j.ijrmms.2004.03.032

Francioni M, Antonaci F, Sciarra N, et al (2020) Application of Unmanned Aerial Vehicle Data and Discrete Fracture Network Models for Improved Rockfall Simulations. *Remote Sens* 12:2053. DOI:10.3390/rs12122053

Frattini P, Crosta GB, Agliardi F (2012) Rockfall characterization and modeling. Içinde: Clague JJ, Stead D (ed) *Landslides*. Cambridge University Press, Cambridge, ss 267–281

Frattini P, Crosta GB, Agliardi F, Imposimato S (2013) Landslide Science and Practice. Içinde: Margottini C, Canuti P, Sassa K (ed) Landslide Science and Practice; Challenging Calibration in 3D Rockfall Modelling. Springer Berlin Heidelberg, Berlin, Heidelberg, ss 169–175

Geniş M, Sakız U, Çolak Aydıner B (2017) A stability assessment of the rockfall problem around the Gökgöl Tunnel (Zonguldak, Turkey). *Bull Eng Geol Environ* 76:1237–1248. DOI:10.1007/s10064-016-0907-1

Giordan D, Baldo M, Guzzetti F, et al (2019) Brief communication: Remotely piloted aircraft systems for rapid emergency response: Road exposure to rockfall in Villanova di Accumoli (central Italy). *Nat Hazards Earth Syst Sci* 19:325–335. DOI:10.5194/nhess-19-325-2019

Giordan D, Manconi A, Facello A, et al (2015) Brief Communication: The use of an unmanned aerial vehicle in a rockfall emergency scenario. *Nat Hazards Earth Syst Sci* 15:163–169. DOI:10.5194/nhess-15-163-2015

Gomez C, Purdie H (2016) UAV- based Photogrammetry and Geocomputing for Hazards and Disaster Risk Monitoring – A Review. Geoenvironmental Disasters 3:. DOI:10.1186/s40677-016-0060-y

Graber A, Santi P (2022) Power law models for rockfall frequency-magnitude distributions: review and identification of factors that influence the scaling exponent. *Geomorphology* 418:108463. DOI:10.1016/j.geomorph.2022.108463

Gül M, Özbek A, Karacan E (2016) Rock fall hazard assessment in Asar Hill, ancient Mabolla City, Mugla—SW Turkey. *Environ Earth Sci* 75:1310. DOI:10.1007/s12665-016-6113-4

Guzzetti F, Crosta G, Detti R, Agliardi F (2002) STONE: A computer program for the three-dimensional simulation of rock-falls. C*omput Geosci* 28:1079–1093. DOI:10.1016/S0098-3004(02)00025-0

Hungr O, Leroueil S, Picarelli L (2014) The Varnes classification of landslide types, an update. Landslides 11:167–194. DOI:10.1007/s10346-013-0436-y

Jaboyedoff M, Labiouse V (2011) Technical note: Preliminary estimation of rockfall runout zones. Nat Hazards Earth Syst Sci 11:819–828. DOI:10.5194/nhess-11-819-2011

Kayabaşı A (2018) The assesment of rockfall analysis near a railroad: a case study at the Kızılinler village of Eskişehir, Turkey. Arab J Geosci 11:800. DOI:10.1007/s12517-018-4175-1

Kazancı N (2020) Kapadokya'nın arazi yapısı ve sınırları, Türkiye. Türkiye Jeol Bülteni / Geol Bull Turkey 1–8. DOI:10.25288/tjb.695327

Keskin İ, Polat A (2022) Kinematic Analysis and Rockfall Assessment of Rock Slope at the UNESCO World Heritage city (Safranbolu/Turkey). Iran J Sci Technol Trans Civ Eng 46:367–384. DOI:10.1007/s40996-021-00803-8

Kim DH, Gratchev I, Berends J, Balasubramaniam A (2015) Calibration of restitution coefficients using rockfall simulations based on 3D photogrammetry model: a case study. Nat Hazards 78:1931–1946. DOI:10.1007/s11069-015-1811-x

Koukouvelas I, Litoseliti A, Nikolakopoulos K, Zygouri V (2015) Earthquake triggered rock falls and their role in the development of a rock slope: The case of Skolis Mountain, Greece. Eng Geol 191:71–85. DOI:10.1016/j.enggeo.2015.03.011

Koukouvelas I, Nikolakopoulos KG, Zygouri V, Kyriou A (2020) Post-seismic monitoring of cliff mass wasting using an unmanned aerial vehicle and field data at Egremni, Lefkada Island, Greece. *Geomorphology* 367:107306. DOI:10.1016/j.geomorph.2020.107306

Lan H, Derek Martin C, Lim CH (2007) RockFall analyst: A GIS extension for three-dimensional and spatially distributed rockfall hazard modeling. Comput Geosci 33:262–279. DOI:10.1016/j.cageo.2006.05.013

Leine RI, Schweizer A, Christen M, et al (2014) Simulation of rockfall trajectories with consideration of rock shape

Li L, Lan H (2015) Probabilistic modeling of rockfall trajectories: a review. Bull Eng Geol Environ 74:1163–1176. DOI:10.1007/s10064-015-0718-9

Liu G, Li J, Wang Z (2021) Experimental Verifications and Applications of 3D-DDA in Movement Characteristics and Disaster Processes of Rockfalls. *Rock Mech Rock Eng.* DOI:10.1007/s00603-021-02394-2

Loye A, Jaboyedoff M, Pedrazzini A (2009) Identification of potential rockfall source areas at a regional scale using a DEM-based geomorphometric analysis. *Nat Hazards Earth Syst Sci* 9:1643–1653. DOI:10.5194/nhess-9-1643-2009

Lu G, Caviezel A, Christen M, et al (2019) Modelling rockfall impact with scarring in compactable soils. *Landslides* 16:2353–2367. DOI:10.1007/s10346-019-01238-z

Manconi A, Ziegler M, Blöchliger T, Wolter A (2019) Technical note: optimization of unmanned aerial vehicles flight planning in steep terrains. *Int J Remote*

Sens 40:2483–2492. DOI:10.1080/01431161.2019.1573334

Mary Vick L, Zimmer V, White C, et al (2019) Significance of substrate soil moisture content for rockfall hazard assessment. *Nat Hazards Earth Syst Sci* 19:1105–1117. DOI:10.5194/nhess-19-1105-2019

Matasci B, Jaboyedoff M, Loye A, et al (2015) Impacts of fracturing patterns on the rockfall susceptibility and erosion rate of stratified limestone. *Geomorphology* 241:83–97. DOI:10.1016/j.geomorph.2015.03.037

Michoud C, Derron M, Horton P, et al (2012) Rockfall hazard and risk assessments along roads at a regional scale : example in Swiss Alps. 615–629. DOI:10.5194/nhess-12-615-2012

Monsalve JJ, Pfreundschuh A, Soni A, Ripepi N (2021) Automated Discontinuity Extraction Software Versus Manual Virtual Discontinuity Mapping: Performance Evaluation in Rock Mass Characterization and Rockfall Hazard Identification. *Mining, Metall Explor* 38:1383–1394. DOI:10.1007/s42461-021-00416-9

Nasery MM, Cosgun SI, Temel BA (2022) Multi-Scenario Analysis of Rockfall Hazard for a Historical Vaulted Masonry Building in Sumela Monastery. *Int J Archit Herit* 1–29. DOI:10.1080/15583058.2022.2091967

Noël F, Jaboyedoff M, Caviezel A, et al (2022) Rockfall trajectory reconstruction: a flexible method utilizing video footage and high-resolution terrain models. *Earth Surf Dyn* 10:1141–1164. DOI:10.5194/esurf-10-1141-2022

Öztürk MZ, Çetinkaya G, Aydın S (2017) Köppen-Geiger İklim Sınıflandırmasına Göre Türkiye'nin İklim Tipleri. *Coğrafya Derg* 17-27 (In Turkish)

Pérez-Rey I, Riquelme A, González-deSantos LM, et al (2019) A multi-approach rockfall hazard assessment on a weathered granite natural rock slope. *Landslides* 16:2005–2015. DOI:10.1007/s10346-019-01208-5

Riquelme A, Cano M, Tomás R, Abellán A (2017) Identification of Rock Slope Discontinuity Sets from Laser Scanner and Photogrammetric Point Clouds: A Comparative Analysis. *Procedia Eng* 191:838–845. DOI:10.1016/j.proeng.2017.05.251

Riquelme A, Tomás R, Cano M, et al (2018) Automatic Mapping of Discontinuity Persistence on Rock Masses Using 3D Point Clouds. Rock Mech *Rock Eng* 51:3005–3028. DOI:10.1007/s00603-018-1519-9

Riquelme AJ, Abellán A, Tomás R, Jaboyedoff M (2014) A new approach for semi-automatic rock mass joints recognition from 3D point clouds. *Comput Geosc*i 68:38–52. DOI:10.1016/j.cageo.2014.03.014

Ritchie AM (1963) Evaluation of Rockfall and Its Control. Highw Res Rec 17, Stab Rock Slopes, Highw Res Board, Natl Res Counc Washington, DC 13–28

Rocscience (2016). Dips An Interactive Analysis of Orientation Based Geological Data Software Program (Version 7); Toronto, ON, Canada, Available online: http://www.rocscience.com.

Rodriguez J, Macciotta R, Hendry MT, et al (2020) UAVs for monitoring, investigation, and mitigation design of a rock slope with multiple failure mechanisms—a case study. *Landslides* 17:2027–2040. DOI:10.1007/s10346-020-01416-4

Sarro R, Carlos J, Mar R (2018) Rockfall Simulation Based on UAV Photogrammetry Data Obtained during an Emergency Declaration : Application at a Cultural Heritage Site. *Remote Sens.* DOI:10.3390/rs10121923

Sazid M (2019) Analysis of rockfall hazards along NH-15: A case study of Al-Hada road. *Int J Geo-Engineering* 10:1–13. DOI:10.1186/s40703-019-0097-3

Schilirò L, Robiati C, Smeraglia L, et al (2022) An integrated approach for the reconstruction of rockfall scenarios from UAV and satellite-based data in the Sorrento Peninsula (southern Italy). *Eng Geol* 308:106795. DOI:10.1016/j.enggeo.2022.106795

Schober A, Bannwart C, Keuschnig M (2012) Rockfall modelling in high alpine terrain - validation and limitations / Steinschlagsimulation in hochalpinem Raum - Validierung und Limitationen. Geomech Tunn 5:368–378. DOI:10.1002/geot.201200025

Sellmeier B, Thuro K (2017) Comparison of two 3D rockfall codes on behalf of a case study in the Bavarian Alps. Geomech und Tunnelbau 10:15–23. DOI:10.1002/geot.201600071

Singh A, Pal S, Kanungo DP (2018) Site-Specific Vulnerability Assessment of Buildings Exposed to Rockfalls. Renew Energy its Innov Technol 1–11. DOI:10.1007/978-981-13-2116-0_1

Taga H, Zorlu K (2016) Assessment of rockfall hazard on the steep-high slopes: Ermenek (Karaman, Turkey). *Nat Hazards Earth Syst Sci Discuss* 1–32. DOI:10.5194/nhess-2015-337

Tamminga A, Hugenholtz C, Eaton B, Lapointe M (2015) Hyperspatial Remote Sensing of Channel Reach Morphology and Hydraulic Fish Habitat Using an Unmanned Aerial Vehicle (UAV): A First Assessment in the Context of River Research and Management. River Res Appl 31:379–391. DOI:10.1002/rra.2743

Tanoli JI, Chen N, Ullah I, et al (2022) Modified "Rockfall Hazard Rating System for Pakistan (RHRSP)": An Application for Hazard and Risk Assessment along the Karakoram Highway, Northwest Pakistan. *Appl Sci* 12:3778. DOI:10.3390/app12083778

Topal T, Akın MK, Akın M (2012) Rockfall hazard analysis for an historical Castle in Kastamonu (Turkey). *Nat Hazards* 62:255–274. DOI:10.1007/s11069-011-9995-1

Török Á, Barsi Á, Bögöly G, et al (2017) Slope stability and rock fall hazard assessment of volcanic tuffs using RPAS and TLS with 2D FEM slope modelling. *Nat Hazards Earth Syst Sci Discuss* 1–30. DOI:10.5194/nhess-2017-56

Torsello G, Vallero G, Castelli M (2021) The role of block shape and slenderness in the preliminary estimation of rockfall propagation. *IOP Conf Ser Earth Environ Sci* 833:012177. DOI:10.1088/1755-1315/833/1/012177

Utlu M, Öztürk MZ, Şimşek M (2021) Yüksek Çözünürlüklü Sayısal Yüzey Modellerine Uygulanan Üç Boyutlu Analizler ile Kaya Düşmelerine Ait Sayısal Risk Değerlendirmesi: Ünlüyaka Köyü (Niğde, Türkiye). Içinde: Döker MF, Akköprü E (ed) COĞRAFYA ARAŞTIRMALARINDA COĞRAFİ

BİLGİ SİSTEMLERİ UYGULAMALARI II, I. PEGEM AKADEMi, Ankara-Turkey, ss 51–69

Utlu M, Öztürk MZ, Şimşek M (2020a) Rockfall analysis based on UAV technology in Kazıklıali Gorge, Aladağlar (Taurus Mountains, Turkey). *Int J Environ Geoinformatics* 7:239–251. DOI:10.30897/ijegeo

Utlu M, Öztürk MZ, Şimşek M (2020b) Emli Vadisi'ndeki (Aladağlar) Talus Depolarının Kantitatif Analizlere Göre İncelenmesi. Içinde: Birinci S, Kıvanç Kaymaz Ç, Kızılkan Y (ed) COĞRAFİ PERSPEKTİFLE DAĞ VE DAĞLIK ALANLAR (Sürdürülebilirlik-Yönetim-Örnek Alan İncelemeleri), I. Kriter Yayınevi, İstanbul-Turkey, ss 51–72

Valkaniotis S, Papathanassiou G, Ganas A (2018) Mapping an earthquake-induced landslide based on UAV imagery; case study of the 2015 Okeanos landslide, Lefkada, Greece. *Eng. Geol.* 245:141–15

Vo DT (2015) RAMMS : Rockfall versus Rockyfor3D in rockfall trajectory simulations at the Community of Vik , Norway Dam Thanh Vo RAMMS :: Rockfall versus Rockyfor3D in rockfall trajectory simulations at the Community of Vik , Norway. University of Oslo, Faculty of Mathematics and Natural Sciences, Master Thesis in Geosciences

Volkwein A, Schellenberg K, Labiouse V, et al (2011) Rockfall characterisation and structural protection - A review. *Nat Hazards Earth Syst Sci* 11:2617–2651. DOI:10.5194/nhess-11-2617-2011

Wang M, Zhou J, Chen J, et al (2023) Automatic identification of rock discontinuity and stability analysis of tunnel rock blocks using terrestrial laser scanning. *J Rock Mech Geotech Eng*. DOI:10.1016/j.jrmge.2022.12.015

Wang W, Zhao W, Chai B, et al (2022) Discontinuity interpretation and identification of potential rockfalls for high-steep slopes based on UAV nap-of-the-object photogrammetry. *Comput Geosci* 166:105191. DOI:10.1016/j.cageo.2022.105191

Wieczorek GF, Morrissey MM, Iovine G, Godt JW (1998) Rock-fall hazards in the Yosemite Valley, California. *U S Geol Surv Open-file Rep* 98–467:

Xu W, Zhang Y, Li X, et al (2020) Extraction and statistics of discontinuity orientation and trace length from typical fractured rock mass: A case study of the Xinchang underground research laboratory site, China. *Eng Geol* 269:105553. DOI:10.1016/ j.enggeo.2020.105553

Yan J, Chen J, Tan C, et al (2023) Rockfall source areas identification at local scale by integrating discontinuity-based threshold slope angle and rockfall trajectory analyses. *Eng Geol* 313:106993. DOI:10.1016/j.enggeo.2023.106993

Yin Y, Li B, Gao Y, et al (2023) Geostructures, dynamics and risk mitigation of high-altitude and long-runout rockslides. *J Rock Mech Geotech Eng* 15:66–101. DOI:10.1016/j.jrmge.2022.11.001

Youssef AM, Pradhan B, Al-Kathery M, et al (2015) Assessment of rockfall hazard at Al-Noor Mountain, Makkah city (Saudi Arabia) using spatio-temporal remote sensing data and field investigation. *J African Earth Sci* 101:309–321. DOI:10.1016/j.jafrearsci. 2014.09.021

Žabota B, Mikoš M, Kobal M (2021) Rockfall Modelling in Forested Areas: The Role of Digital Terrain Model Grid Cell Size. *Appl Sci* 11:1461. DOI:10.3390/app11041461

Zhang L (2006) Rock discontinuities. In: Zhang L (eds) Engineering properties of rocks, 4th edn. Elsevier, A. Içinde: Zhang L (ed) Elsevier., 4th edn. Elsevier, Amsterdam, ss 226–230

Zhang W, Zhao X, Pan X, et al (2022) Characterization of high and steep slopes and 3D rockfall statistical kinematic analysis for Kangyuqu area, China. *Eng Geol* 308:106807. DOI:10.1016/j.enggeo. 2022.106807

Zhang Y, Yue P, Zhang G, et al (2019) Augmented Reality Mapping of Rock Mass Discontinuities and Rockfall Susceptibility Based on Unmanned Aerial Vehicle *Photogrammetry. Remote Sens* 11:1311. DOI:10.3390/rs11111311